Two-dimensional velocity of the magnetic structure observed on 11 July 2017 by the Magnetospheric Multiscale spacecraft

Richard E. Denton [1], Roy B. Torbert [2], Kevin J. Genestreti [3], Hiroshi Hasegawa [4], Roberto Manuzzo [5,6], Gerard Belmont [5], Laurence Rezeau [5], Francesco Califano [6], Rumi Nakamura [7], Jan Egedal [8], Olivier Le Contel [5], James L. Burch [9], Ivan Dors [2], Matthew R. Argall [2], Christopher T. Russell [10], Robert J. Strangeway [10], and Barbara L. Giles [11]

[1]Department of Physics and Astronomy, Dartmouth College, Hanover, New Hampshire, USA
[2]Institute for the Study of Earth, Oceans, and Space, University of New Hampshire, Durham, New Hampshire, USA.
[3]Institute for the Study of Earth, Oceans, and Space, Southwest Research Institute, Durham, New Hampshire, USA.
[4]Institute of Space and Astronautical Science, JAXA, Sagamihara, Japan.
[5]LPP, CNRS, Ecole polytechnique, Sorbonne Université, Observatoire de Paris, Université Paris-Saclay, PSL Research University, Paris, France.
[6]Department of Physics E. Fermi, Università di Pisa, Italia
[7]Space Research Institute, Austrian Academy of Sciences, Graz, Austria.
[8]Department of Physics, University of Wisconsin-Madison, Madison, Wisconsin, USA.
[9]Space Science and Engineering Division Southwest Research Institute, San Antonio, Texas, USA.
[10]Institute of Geophysics and Planetary Physics, University of California at Los Angeles, Los Angeles, California, USA.
[11]NASA Goddard Space Flight Center, Greenbelt, MD, USA.

Key Points:

- We demonstrate use of Spatio-Temporal Difference (STD) and polynomial reconstruction to determine the 2-D velocity of a magnetic structure
- Velocities from STD and reconstruction roughly agree with each other and with estimates from other references for the 11 July 2017 event
- Polynomial reconstruction is only likely to be accurate within a distance of 2 spacecraft spacings from the centroid of the MMS spacecraft

Corresponding author: R. E. Denton, `redenton at dartmouth dot edu`

Abstract

In order to determine particle velocities and electric field in the frame of the magnetic structure, one first needs to determine the velocity of the magnetic structure in the frame of the spacecraft observations. Here, we show how to determine a two dimensional magnetic structure velocity for the magnetic reconnection event observed in the magnetotail by the Magnetospheric Multiscale (MMS) spacecraft on 11 July 2017. We use two different multi-spacecraft methods, Spatio-Temporal Difference (STD) and the recently developed polynomial reconstruction method. Both of these methods use the magnetic field measurements, and the reconstruction technique also uses the current density measured by the particle instrument. We find rough agreement between the results of our methods and with other velocity determinations previously published. We also explain a number of features of STD and show that the polynomial reconstruction technique is only likely to be valid within a distance of two spacecraft spacings from the centroid of the MMS spacecraft. Both of these methods are susceptible to contamination by magnetometer calibration errors.

1 Introduction

In magnetic reconnection, plasma flows toward the magnetic X line (a magnetic null in the reconnection plane, in which it appears as an X point) with an inflow velocity and is accelerated and ejected in an orthogonal direction with an outflow velocity because of the large curvature of the magnetic field in the vicinity of the X line [e.g., *Vasyliunas*, 1975; *Sonnerup*, 1979]. To determine these velocities, one needs to determine the frame of reference in which the X line is stationary. Thus an important part of the process of understanding a magnetic reconnection event is to determine the velocity of the magnetic structure relative to the observing spacecraft. Although on large scales, plasma may be "frozen in" to the magnetic field, at least in directions perpendicular to the magnetic field, this is typically not the case on small scales close to the X line, especially in the region known as the electron diffusion region [*Hesse et al.*, 2011, 2014].

Shi et al. [2019] has recently reviewed methods to determine a coordinate system and magnetic structure velocity. Methods to determine the velocity include calculating the deHoffmann-Teller frame in which the electric field is approximately zero, various types of timing analysis, various reconstruction methods, and the Spatial-Temporal Difference (STD) method [*Shi et al.*, 2006]. STD has been recently used by *Denton et al.* [2016a,b] and *Yao et al.* [2016, 2018] to determine the time-dependent velocity of a magnetic structure in the normal direc-

tion. *Alm et al.* [2017] recently used STD to calculate the time-dependent two-dimensional velocity of the spacecraft moving through a structure of ion-scale magnetopause flux ropes. *Manuzzo et al.* [2019] recently described difficulties with calculating the structure velocity in multiple dimensions, and suggested new approaches to calculate the velocity. Their method includes the possibility of including mild time dependence. The implementation of STD that we will describe in this paper is somewhat simpler, and assumes that the structure velocity is constant on the timescale of motion across the spacecraft separation, as did the original STD.

Recently *Torbert et al.* [2018a, 2020] introduced a new method for reconstruction of the instantaneous magnetic field in the region close to the MMS spacecraft using a polynomial expansion of the magnetic field with input from the spacecraft measurements of the magnetic field and particle current density. *Denton et al.* [2020] described a number of variations of Torbert et al.'s method and tested the validity of the magnetic field model during times in which the magnetic structure was roughly 2 dimensional. In this paper, we will use Denton et al.'s Reduced Quadratic model that results from the assumption that $\lambda_1 \gg \lambda_2 \gg \lambda_3$, where λ_i are the eigenvalues of Minimum Directional Derivative (MDD) analysis that determines the eigenvectors of the gradient of the vector magnetic field [*Shi et al.*, 2005].

We will apply our implementation of STD to calculate the velocity of the magnetic structure for the magnetotail reconnection event on 11 July 2017 described by *Torbert et al.* [2018b]. In the process, we will elucidate several aspects of the method. Then we will use the new polynomial reconstruction method to get a second estimate of the velocity.

The paper is organized as follows. In section 2, we describe the data and methods to be used, in section 3 we calculate the velocity of the magnetic structure using the two methods, and in section 4 we discuss our results, including comparison to previous estimates of the structure velocity from other methods.

2 Data and Methods

2.1 MMS Data

In this paper we will examine the magnetotail reconnection event on 11 July 2017 at 22:34 UT. The time t will be measured in seconds after this time. This event was first studied by Torbert et al. [*Torbert et al.*, 2018b], and has been the subject of a number of other papers [e.g., *Genestreti et al.*, 2018; *Nakamura et al.*, 2019; *Hasegawa et al.*, 2019; *Egedal et al.*, 2019]. The position of the spacecraft was in the magnetotail at [-21.53, 4.23, 3.64] R_E

in geocentric solar ecliptic (GSE) coordinates. The average separation between spacecraft was 18.3 km. We will be concentrating on the interval t =1.6—2.8 s, during which the magnetic structure was moving tailward, so that, relative to that structure, the MMS spacecraft skimmed past the reconnection X line nearly along but below the current sheet.

As discussed by *Denton et al.* [2020], we use the magnetic field and particle current density from the MMS mission [*Burch et al.*, 2015]. The fluxgate magnetometer (FGM) [*Russell et al.*, 2016] and search coil magnetometer (SCM) [*Le Contel et al.*, 2016] data are combined into a single product with original resolution of 0.12 ms [*Fischer et al.*, 2016; *Argall et al.*, 2018]. We boxcar average this to 1 ms resolution. We calculate the particle current density, **J**, from the burst mode ion and electron bulk velocity moments from the Fast Plasma Instrument (FPI) [*Pollock et al.*, 2016], using the formula $\mathbf{J} = en'_e (\mathbf{V}_i - \mathbf{V}_e)$, where e is the proton charge, n'_e is an adjusted electron density, and $\mathbf{V}_i$ and $\mathbf{V}_e$ are respectively the ion and electron bulk velocity. Within the time interval 1.6 s to 3.1 s (a slightly more complete time interval than the one we will analyze), a factor f is found at each time step such that $fn_e (\mathbf{V}_i - \mathbf{V}_e)$ averaged over the spacecraft is closest in a least-squares sense to the current density from the "curlometer" [*Robert et al.*, 1998] technique, that determines the current density from $\nabla \times \mathbf{B}/\mu_0$ using the spacecraft **B** values and spatial separations. During this time interval, the values of f varied between 0.65 and 1.13. The quantity n'_e is the median value of f for the time series, 0.844, multiplied by the observed n_e. This adjustment was made because $\mathbf{J}_{curl}$ is considered to be more accurate than **J**; but using the constant in time median value of f allowed for the possibility of real time variation of **J** averaged over the spacecraft.

The resolution of the electron moments was 30 ms, and that of the ions (measured collectively) was 150 ms. These are interpolated to 1 ms resolution. Though we keep the data at this resolution, the effective time resolution is much less, since we here boxcar average the data to 0.5 s resolution. Despite this smoothing, use of the combined FGM/SCM magnetometer product reduces noise relative to that found using the burst mode data, probably by reducing the error associated with interpolating the individual MMS spacecraft field values (with different timestamps) to common times.

Because of this averaging, our methods are likely to be accurate only in some average sense on a timescale $\leq$ 0.5 s. Our reconstruction technique has previously revealed some significant time dependence [*Denton et al.*, 2020], and we find time variation in the structure

velocity also here using both STD and the polynomial reconstruction (Figure 3a). There may very well be more detailed short timescale behavior that we do not describe.

2.2 Structure velocity from STD

The Spatio-Temporal Difference (STD) method of *Shi et al.* [2006] is based on the convection equation,

$$\frac{d\mathbf{B}}{dt} = \frac{\partial \mathbf{B}}{\partial t} + \mathbf{V}_{sc} \cdot \nabla \mathbf{B}, \tag{1}$$

where $\mathbf{V}_{sc}$ is the velocity of the spacecraft relative to the magnetic structure and $d\mathbf{B}/dt$ is the rate of change of the magnetic field observed at the spacecraft. Shi et al. neglected the partial time derivative relative to the convective term to get

$$\frac{d\mathbf{B}}{dt} = -\mathbf{V}_{str} \cdot \nabla \mathbf{B}, \tag{2}$$

where $\mathbf{V}_{str} = -\mathbf{V}_{sc}$ is the structure velocity relative to the spacecraft. This equation can be solved as a set of simultaneous equations at the resolution of the magnetometer data, yielding time-dependent structure velocities.

Assume that an event *L*-*M*-*N* coordinate system has been established [*Denton et al.*, 2018; *Genestreti et al.*, 2018, and references therein]. Usually we want *L* to be the direction of the reconnection magnetic field; *N* may be the normal direction across the current sheet, and *M* is the other direction. In the common two dimensional description of magnetic reconnection, *M* is assumed to be the direction of invariance, but sometimes the most invariant direction has a different orientation than that of *M* if the *L* direction is determined based on maximum variance of **B** [*Denton et al.*, 2016a, 2018].

A local time-dependent coordinate system *l*-*m*-*n* is based on the eigenvectors of Minimum Directional Derivative (MDD) analysis [*Shi et al.*, 2005]. In MDD, a symmetric tensor is formed by multiplying the gradient of the vector magnetic field by its transpose, and then the eigenvectors of the resulting symmetric tensor are found. In this case, *n* is the maximum gradient direction, *m* is the minimum gradient direction, and *l* is the intermediate gradient direction. (The definitions of *l* and *m* are reversed from those recently used by *Manuzzo et al.* [2019].) If the coordinate system is time invariant, *l*-*m*-*n* would be the same as the event coordinate system *L*-*M*-*N* if the gradient is a minimum in the *M* direction.

As described by *Shi et al.* [2006], and further in Appendix A, we can solve (2) for the local gradient $k = l$, m, or n component of the structure velocity, $\mathcal{V}_{\mathrm{str,k}}$, using

$$\mathcal{V}_{\mathrm{str,k}} = -\mathcal{B}_{dt,i}\ \mathcal{G}_{k,i}\ /\ \lambda_k, \tag{3}$$

where $\mathcal{B}_{dt,i}$ is the i component of the time derivative of $\mathbf{B}$ as observed by the spacecraft, $\mathbf{G} = \nabla\mathbf{B}$, λ_k is one of the MDD eigenvalues, the calligraphy letters indicate that the quantities are in the local gradient (l-m-n) coordinates system, and repeated indices are summed. Expanding this out explicitly,

$$\mathcal{V}_{\mathrm{str},k} = -\frac{1}{\lambda_k}\left(\frac{d\mathcal{B}_n}{dt}\frac{\partial\mathcal{B}_n}{\partial\mathcal{X}_k} + \frac{d\mathcal{B}_l}{dt}\frac{\partial\mathcal{B}_l}{\partial\mathcal{X}_k} + \frac{d\mathcal{B}_m}{dt}\frac{\partial\mathcal{B}_m}{\partial\mathcal{X}_k}\right), \tag{4}$$

where $\mathcal{X}$ is the position vector in the MDD eigenvector frame. From (4), we see that the dominant source of $\mathcal{V}_{\mathrm{str},k}$ is from the term $\mathcal{B}_i$ for which the product of its time derivative and spatial gradient in the $\mathcal{X}_k$ direction is the greatest.

For example, suppose that we can define a reconnection L-M-N coordinate system for which the largest variation is for B_L and the largest spatial variation is in the N direction [*Denton et al.*, 2018]. Then $\lambda_n \approx (\partial B_L/\partial X_N)^2$, and (4) would become

$$V_{\mathrm{str},N} \approx -\frac{(dB_L/dt)\,(\partial B_L/\partial X_N)}{(\partial B_L/\partial X_N)^2} \sim -\frac{dX_N}{dt}. \tag{5}$$

(The minus sign is because the left-hand side of (5) is the structure velocity, but dX_N/dt on the right hand side of (5) is the time derivative of the spacecraft displacement relative to the structure.)

In the following text, we will drop the calligraphy notation, so, for instance, $V_{\mathrm{str},n}$ is the structure velocity in the local MDDB n direction.

2.3 Reduced quadratic polynomial reconstruction model

As discussed by *Denton et al.* [2020], the 3D Reduced quadratic (RQ-3D) model was found by starting with the full quadratic expansion, and then reducing the number of terms based on the ordering $\partial/\partial n \gg \partial/\partial l \gg \partial/\partial m$. Because $\partial/\partial m$ is assumed to be small, we only allow "strictly linear" variation with respect to m. That is, the m-dependent terms are linear in m, and do not have l or n dependence. Then the m derivatives will be everywhere constant and therefore no greater than those determined from the linear gradients based on the MMS inter-spacecraft magnetic field variation. Because $\partial/\partial n$ is big, we also expect $\partial B_n/\partial n$ to be small because of $\nabla\cdot\mathbf{B} = 0$, so we also neglect $\partial^2 B_n/\partial n^2$ to ensure that $\partial B_n/\partial n$

remain small away from the spacecraft. This leads to neglect of other terms, as described in more detail by *Denton et al.* [2020]. The resulting model is

$$B_l = B_{l,0} + \frac{\partial B_l}{\partial n} n + \frac{\partial B_l}{\partial l} l + \frac{\partial B_l}{\partial m} m + \frac{\partial^2 B_l}{\partial n^2} \frac{n^2}{2} \tag{6}$$

$$B_m = B_{m,0} + \frac{\partial B_m}{\partial n} n + \frac{\partial B_m}{\partial l} l + \frac{\partial B_m}{\partial m} m + \frac{\partial^2 B_m}{\partial n^2} \frac{n^2}{2} + \frac{\partial^2 B_m}{\partial n \partial l} nl + \frac{\partial^2 B_m}{\partial l^2} \frac{l^2}{2} \tag{7}$$

$$B_n = B_{n,0} + \frac{\partial B_n}{\partial n} n + \frac{\partial B_n}{\partial l} l + \frac{\partial B_n}{\partial m} m + \frac{\partial^2 B_n}{\partial l^2} \frac{l^2}{2} \tag{8}$$

Neglecting the displacement current in the Ampere-Maxell law, $\mu_0 \mathbf{J}$ is the curl of (6–8), which is written out in Appendix B. (Here μ_0 is the permeability of free space.)

In addition to these equations, we have a constraint in order to ensure $\nabla \cdot \mathbf{B} = 0$. Taking the divergence of (6–8), we find

$$\frac{\partial B_n}{\partial n} + \frac{\partial B_l}{\partial l} + \frac{\partial B_m}{\partial m} = 0 \tag{9}$$

The three equations in (6–8) can be solved at each spacecraft location, leading to 12 equations. Similarly the equations for $\mu_0 \mathbf{J}$ in Appendix B also yield 12 equations. With (9), there are a total of 25 equations that can be used to solve for 17 parameters for a best least-squares fit. A more detailed description of the method is given by *Denton et al.* [2020].

3 Results

3.1 MDD analysis

Figure 1 shows the results of Minimum Directional Derivative (MDD) and Minimum Gradient Analysis (MGA), both applied to the vector magnetic field [*Shi et al.*, 2019]. Figure 1a shows the eigenvalues for MDDB, which are also the same as the eigenvalues for MGAB. (MGA will be described below.) Figure 1b–d shows the local (time-dependent) MDDB eigenvectors l, m, and n, respectively, expressed in terms of the global coordinates that we have chosen for this event, L-M-N. As one can see from Figure 1b—d, l, m, and n are approximately equal to L, M, and N, respectively. In fact, $\mathbf{e}_N$ and $\mathbf{e}_M$ were found by taking the mean components of $\mathbf{e}_n$ and $\mathbf{e}_m$, making a slight adjustment of $\mathbf{e}_M$ so that it was perpendicular to $\mathbf{e}_N$, and then getting $\mathbf{e}_L$ from the cross product, $\mathbf{e}_M \times \mathbf{e}_N$. The local $\mathbf{e}_n$ direction is found from the maximum gradient eigenvector, representing the direction of the maximum gradient across the current sheet. The local $\mathbf{e}_m$ direction was the direction of the minimum gradient, so that an approximate two-dimensional representation of this system would include variation only in the N and L directions.

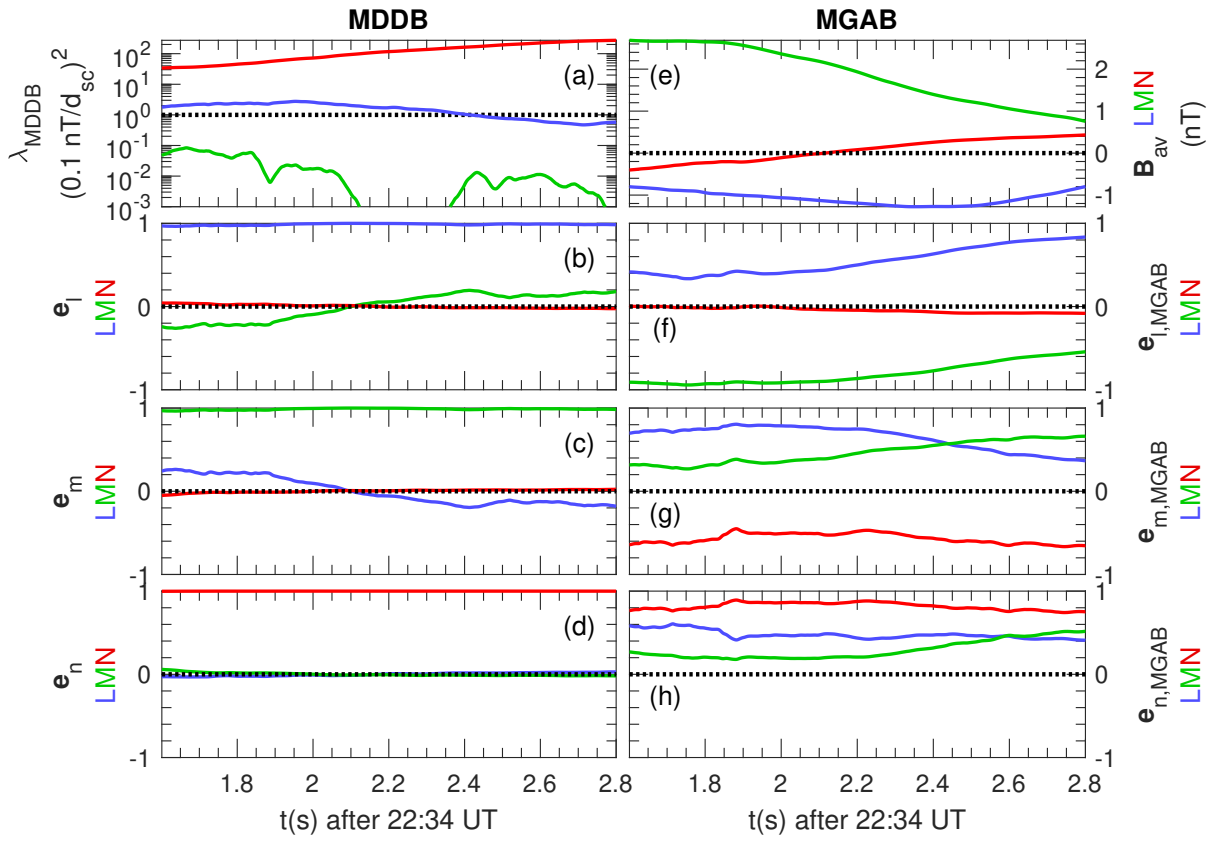

Figure 1. Minimum Directional Derivative (MDD) and Minimum Gradient Analysis (MGA). (a) MDDB (or MGAB) eigenvalues; (b—d) local MDDB *l*, *m*, and *n* eigenvectors, respectively, with blue, green, and red curves showing the *L*, *M*, and *N* components, where [*L*;*M*;*N*] = [0.876,0.424,-0.230;-0.476,0.835,-0.275;0.075,0.351,0.936]; (e) *L*-*M*-*N* components of the magnetic field averaged over the MMS spacecraft; (f—h) local MGAB eigenvectors in the same format as for MDDB.

Note that the l and L directions might not well represent the Minimum Variance Analysis (MVA) direction of maximum variance of the magnetic field [*Sonnerup and Cahill*, 1967; *Sonnerup and Scheible*, 1998], which is often associated with L [e.g. *Denton et al.*, 2018]. MGA is a local version of MVA [*Shi et al.*, 2019] that uses the magnetic gradient matrix at one particular time, as does MDD. But MGA compares the values of **B** observed by the four spacecraft to find the components of **B** that have the most or least variation. That is, while MDD finds the directions of largest and least gradient, MGA finds the directions of largest and least variance. In Figure 1f–1h, $\mathbf{e}_{l,\mathrm{MGAB}}$, $\mathbf{e}_{m,\mathrm{MGAB}}$, and $\mathbf{e}_{n,\mathrm{MGAB}}$ are respectively the local MVA-like maximum, intermediate, and minimum variance directions. Figure 1f shows that $\mathbf{e}_{l,\mathrm{MGAB}}$ is at first mostly in the $-M$ direction (green curve with largest absolute value). Later in the interval, there is more variation in the L direction (blue curve with largest absolute value).

We will at first examine this event using the L-M-N coordinate system based on MDDB as described above, with [L; M; N] = [0.879,0.419,-0.230; -0.472,0.837,-0.277; 0.077,0.352,0.933]. These coordinate directions differ by 15°, 16°, and 7°, respectively, from the L, M, and N directions of *Torbert et al.* [2018b], and by 40°, 39°, and 11°, respectively, from the hybrid MDD-B/MVA-v_e L, M, and N directions of *Genestreti et al.* [2018] (coordinate system 14 in their Table A1).

3.2 Velocity from STD

Equation (4) shows that the kth component of the structure velocity in the local MDDB cordinates, $V_{\mathrm{str},k}$ ($\mathcal{V}_{\mathrm{str,k}}$ in (4)), has the kth eigenvalue, λ_k, in the denominator. Thus very small values of λ_k can lead to very large values of the corresponding velocity component. In principle, if the structure were truly two-dimensional and time invariant, and λ_k became very small, the numerator of (4) would also become very small, so that the resulting velocity would be well behaved. But in practice, non-two dimensionality, time dependence, and approximations and errors in the calculation of the gradients can result in small values of the denominator without correspondingly small values of the numerator. Thus very small λ_k yields what we call a "singularity", leading to unrealistically large $V_{\mathrm{str},m}$ [see discussion by *Shi et al.*, 2019; *Manuzzo et al.*, 2019].

Since the relative DC magnetometer calibration of the MMS spacecraft is rated to be accurate to 0.1 nT, values of λ_k below $\lambda_0 = (0.1\ \mathrm{nT}/d_\mathrm{sc})^2$, where d_sc is the average spacecraft

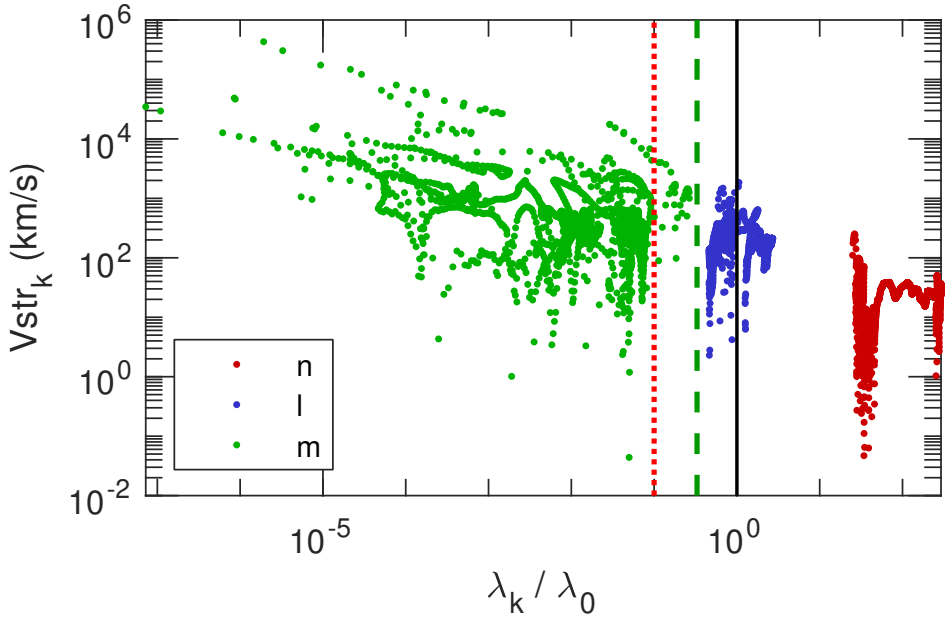

Figure 2. Velocity components in the local MDDB directions versus eigenvalue. The velocity components, $V_{\mathrm{str,k}}$, for the interval t = 1.6 s to 2.8 s are plotted versus the local normalized MDDB eigenvalue, λ_k/λ_0, for the maximum gradient n component (red dots), the intermediate gradient l component (blue dots), and the minimum gradient m component (green dots), where $\lambda_0 = (0.1\ \mathrm{nT}/L_{sc})^2$. The vertical dashed green and dotted red lines are at values of λ_k/λ_0 equal to 0.33 and 0.1, respectively.

spacing (here, 18.3 km), could be suspect [*Shi et al.*, 2019]. Calibration errors are especially serious, because they can lead to systematic (constant) error in the gradients. Figure 2 shows components of the STD structure velocity, $V_{\mathrm{str,k}}$, in the local MDDB eigenvector directions versus the normalized eigenvalue, λ_k/λ_0. One evidence that the gradient in a direction is not being calculated accurately would be that the inferred structure velocity, $V_{\mathrm{str,k}}$, increases as λ_k decreases. This is because, in principle, there should not be any correlation between the velocity in a certain direction and the gradient of the magnetic field in that same direction.

Evidence of this can be seen in Figure 2. Note that the velocities of the minimum gradient component of the structure, $V_{\mathrm{str,min}}$ (green dots), increase with decreasing λ_k/λ_0 for $\lambda_k/\lambda_0 < 10^{-1}$, that is, for data points to the left of the red vertical dotted line in Figure 2. However, there is no indication that the velocities increase with respect to decreasing λ_k/λ_0 for larger eigenvalues than about $\lambda_k/\lambda_0 = 0.25$. For the time being, we are going to proceed with the assumption that the velocities measured in the intermediate gradient direction (blue points in Figure 2) are accurate. This is equivalent to assuming that eigenvalues, λ_k/λ_0, are accurately calculated if their values are greater than 0.33, that is, for data points to the right of the vertical green dashed line in Figure 2. Note also that our main attention will be for the velocity before about 2.2 s, for which λ_l/λ_0 is above unity (Figure 1a).

Figure 3 shows the results of the STD analysis. The solid curves in Figure 3a show the components of the 2D STD magnetic structure velocity formed by projection of the local n and l components onto the global N (red solid curve) and L (blue solid curve) directions. The black curves in Figures 3b—d are the n, l, and m components of the structure velocity, respectively. Comparison of the black curve in Figure 3b with the red curve in Figure 3a, and the black curve in Figure 3c with the blue curve in Figure 3a, shows that the n and l components of the STD velocity are nearly equal to the N and L components, respectively, as suggested by Figure 1d and 1b, respectively. The red, blue, and green curves in Figures 3b—d show the contributions to $V_{str,k}$ for $k = n$, l, or m from the B_n, B_l, and B_m dependent terms, respectively, in (4). As indicated by the very large values of $V_{str,m}$ in Figure 2, $V_{str,m}$ is often grossly inaccurate if the MDDB eigenvalue is very small. Figure 3d, which shows a singularity in $V_{str,m}$, is included only to remind the reader of this fact.

Figures 3b and 3c show some possibly unexpected results. If the spacecraft cross the entire current sheet, often the largest magnetic variation is in the B_L component, due to the strong dependence of B_L on N. Then one would expect the value of $V_{str,n}$ to be dominated

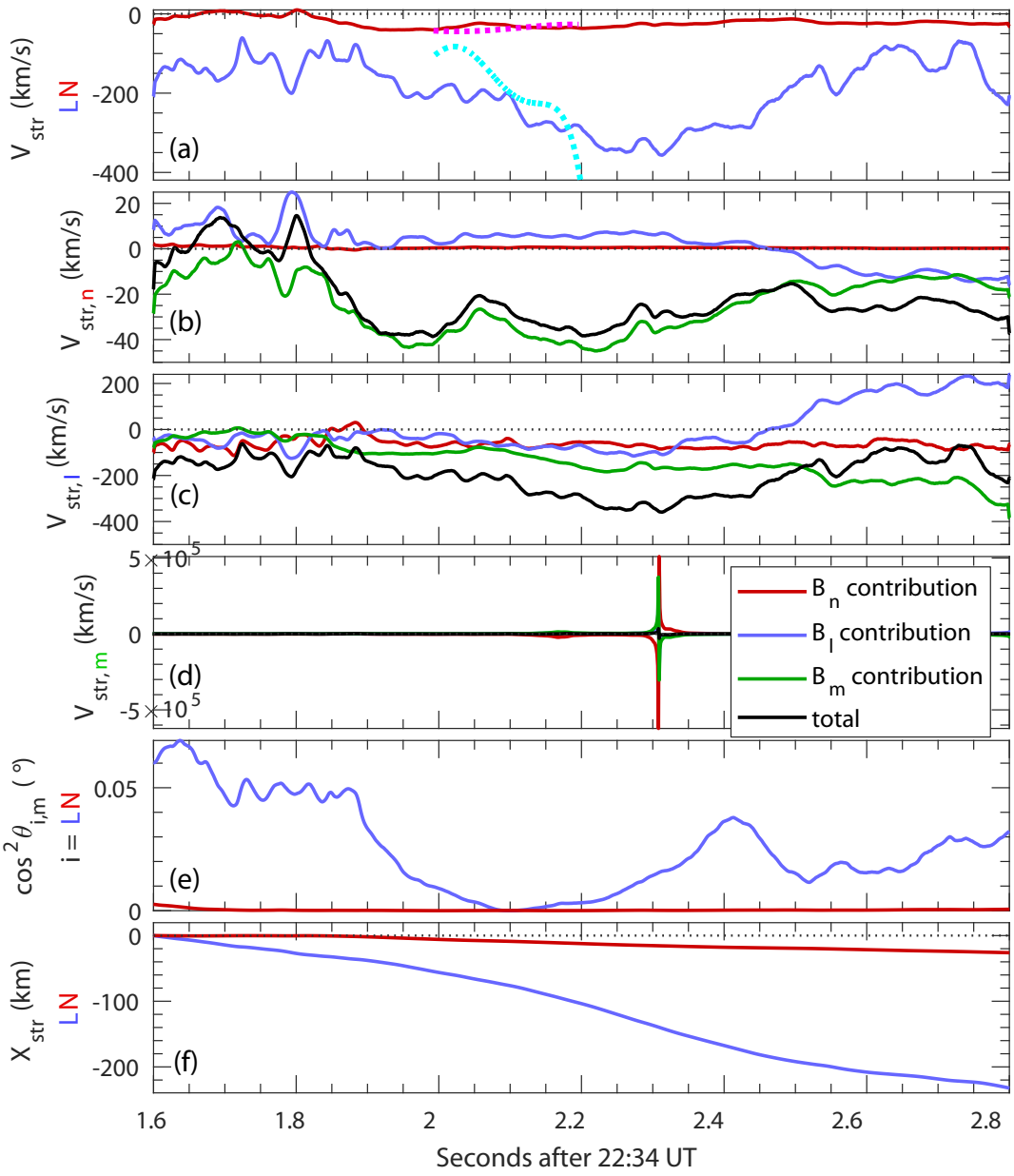

Figure 3. Spatial-Temporal Difference (STD) results. (a) STD velocity components in the L (blue solid curve) and N (red solid curve) directions calculated using only contributions from the MDDB local n and l directions; (b–d) STD velocity component in the MDDB local (b) n, (c) l, and (d) m directions, where the black curve is the total component $V_{str,k}$ for k = n, l, or m, and the red, blue, and green curves are the contributions to $V_{str,k}$ from the B_n, B_l, and B_m terms in (4), respectively; (e) squared cosine of the angle between the L (blue curve) or N (red curve) direction and the m direction; (f) net STD displacement from t = 1.6 s in the L (blue curve) and N (red curve) directions. The dotted curves in Figure 3a are the L (cyan curve) and N (magenta curve) velocity components found from RQ-3D reconstruction during the time when the centroid of the MMS spacecraft was within two average spacecraft separations, d_{sc}, from the X line of the magnetic structure.

by the contribution from the B_L-dependent terms in (4), as was assumed in the derivation of (5). But Figure 3b shows that the value of $V_{str,n}$ is dominated by the contribution from the B_m-dependent terms in (4). This is because for this event the MMS spacecraft were skimming close to but under the current sheet [*Torbert et al.*, 2018b; *Hasegawa et al.*, 2019], so that there was little variation in B_L over the time plotted in Figure 3. From Figure 1e, we can see that B_m is larger in magnitude than B_l, and that the variation in B_m is also larger, except at the end of the time interval after about $t = 2.6$ s. Consequently, $V_{str,n}$ is dominated by the contributions from the B_m-dependent terms in (4) (green curve in Figures 3b) up until about $t = 2.6$ s, after which the B_l-dependent terms also contribute significantly (blue curve in Figures 3b).

Similarly, in the frame of reference of the magnetic structure, if we define $L = 0$ as the L position of the X line, then B_n should change sign across $L = 0$. So one might think that the B_n-dependent terms in (4) would make the greatest contribution to $V_{str,l}$. But B_n is small (Figure 1e), and the greatest contributions to $V_{str,l}$ come from the B_m and B_l-dependent terms in (4) (green and blue curves in Figures 3c, respectively).

The magnitude of $V_{str,i}$, where $i = L$ or N, can be found from the magnitudes of $V_{str,k}$, where $k = l$, m, or n, using

$$V_{str,i} = \sqrt{\cos^2\left(\theta_{i,n}\right) V_{str,n}^2 + \cos^2\left(\theta_{i,l}\right) V_{str,l}^2 + \cos^2\left(\theta_{i,m}\right) V_{str,m}^2}, \tag{10}$$

where $\cos\left(\theta_{i,k}\right)$ is the angle between the i (L or N) and k (l, m, or n) directions. Figure 3e shows $\cos^2\theta_{i,m}$ for $i = L$ (blue curve) and $i = N$ (red curve). Because these values are small, especially for $i = N$, the neglect of $V_{str,m}$ in the calculation of $V_{\mathrm{str},N}$ leads to almost no inaccuracy, and the neglect of $V_{\mathrm{str},m}$ in the calculation of $V_{\mathrm{str},L}$ is not a significant problem unless $V_{\mathrm{str},m} \gg V_{\mathrm{str},l}$. But Figure 2 shows that $V_{\mathrm{str},m}$ (green dots) does not become much greater than $V_{\mathrm{str},l}$ unless the minimum eigenvalue λ_{min} becomes very small ($< 0.1\lambda_0$), for which $V_{\mathrm{str},m}$ is not expected to be accurate. Therefore, our STD values of $V_{\mathrm{str},N}$ should be very accurate, and despite the fact that λ_{int} in Figure 1a (blue curve) is not always above our desired value for accuracy (dotted black line), there are indications that $V_{\mathrm{str},L}$ may be accurate. These include the fact that neither the maximum or intermediate gradient components of $V_{\mathrm{str},k}$ increase with decreasing eigenvalue in Figure 2, and the comparison with the velocity calculated from reconstruction described below.

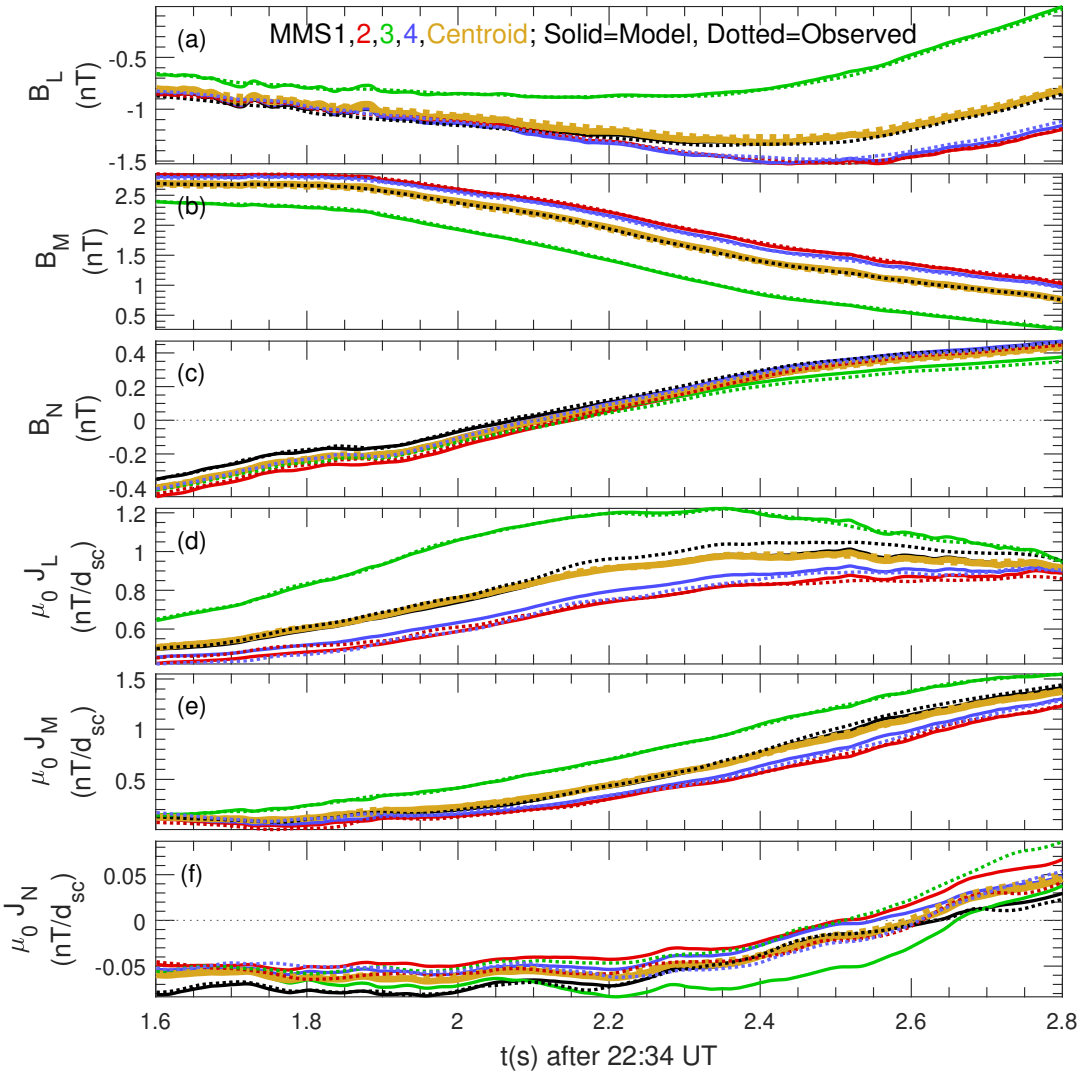

Figure 4. Model and observed magnetic field and current density. (a–c) observed (dotted curves) and RQ-3D model (solid curves) L, M, and N components of **B** for the individual MMS spacecraft, using the colors in the key of panel a; and (d–f) the particle current density **J** using the same colors and line styles as for **B**. The gold curves are the average of the observed values (dotted curves) and the model values at the centroid of the spacecraft positions (solid curves).

3.3 Polynomial reconstruction

Figure 4 shows that the RQ-3D polynomial model well represents **B** and **J** during the time interval $t = 1.6$ s to 2.8 s. The J_N component is not as well modeled as the other components, but it is very small compared to the other components of **J**. This shows that the model is reasonable in the vicinity of the spacecraft, though it does not necessarily show that the model is accurate away from the spacecraft.

Figure 5 shows reconstruction results for the magnetic field in the L–N plane at $M = 0$, where here L, M, and N are measured with respect to the centroid of the MMS spacecraft, at the origin in Figures 5b–5q. The reconstruction appears to show a reconnection X line (extending normal to the L–N plane, so that it is an X point in that plane), indicated by the gold asterisk, that appears slightly after $t = 1.6$ s. The X line does not move much until about $t = 1.92$ s. Then between $t = 1.92$ s and 2.24 s it moves rapidly in the minus L direction relative to the spacecraft. Later, it reappears near the left (negative L) side of the plot from $t = 2.4$ s to 2.8 s. While the L position of the X line is somewhat variable, the X line appears to move uniformly in the minus N direction relative to the spacecraft.

3.4 Path of the spacecraft through the magnetic structure

Figures 6a and 6b show the motion of the reconnection X line relative to the centroid of the MMS spacecraft in the L and N directions, respectively, based on the RQ-3D polynomial reconstruction using data such as in Figure 5. At each time, the position in the L-N plane is found where the in-plane magnetic field is a minimum (indicated by the gold asterisks in Figure 5b—q). (There are also minima corresponding to reconnection O points, but these have been removed from Figure 6.)

The red curve in Figure 6c makes use of the positions from Figures 6a and 6b to show the path of the centroid of the MMS spacecraft relative to the X line, which is at the origin of Figure 6c. The L_{MMS} and N_{MMS} components in Figure 6c have been converted to km using $d_{\mathrm{sc}} = 18.3$ km. The path progresses generally from the left to the right, starting at the black circle. There are some reversals with respect to time of the velocity in the L direction, v_L, at positions indicated by the black arrows. At these positions, all outside a radius of 2 spacecraft spacings (2 d_{sc}) as indicated by the solid green curve, the reconnection X line seems to linger near the periphery of the reconstruction (at a distance of about 2—3 d_{sc}).

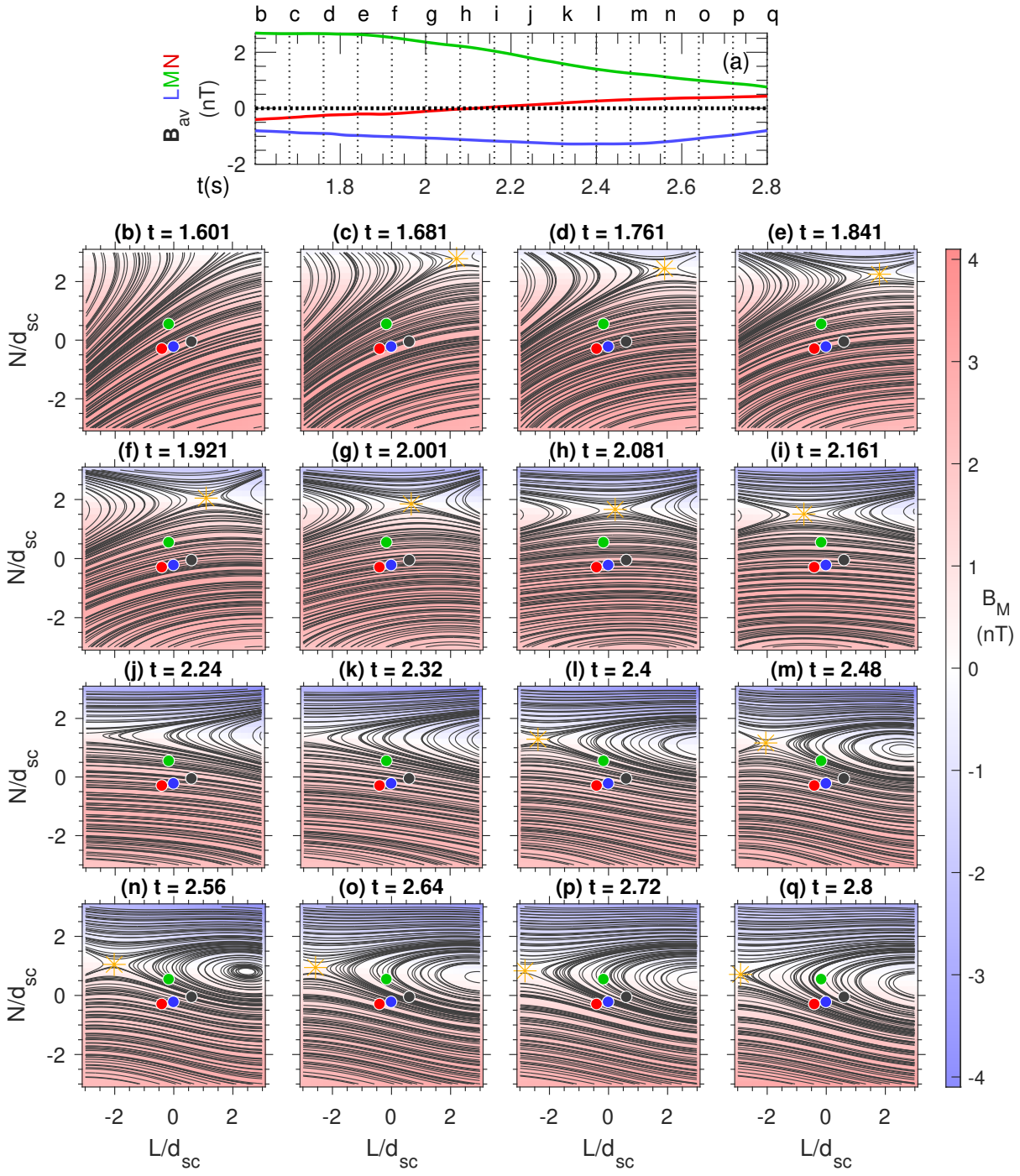

Figure 5. RQ-3D reconstruction of the magnetic field in the L–N plane at $M = 0$. (a) The magnetic field averaged over the spacecraft, $\mathbf{B}_{\text{av}}$; and (b–q) streamlines of the in-plane magnetic field at $M = 0$ (black curves) and B_M (color) for B_M directed into the page using the color scale at the right side of the plot. Each plot is generated at the time indicated in the panel label corresponding to the time of the same label in panel a. The coordinates L and N are measured relative to the centroid of the MMS spacecraft (at the origin of each panel), and the positions of the MMS spacecraft are indicated by the colored circles for MMS1 (black circle), MMS2 (red circle), MMS3 (green circle), and MMS4 (blue circle). The gold asterisks are the position of the X line determined from the in-plane magnetic field minimum.

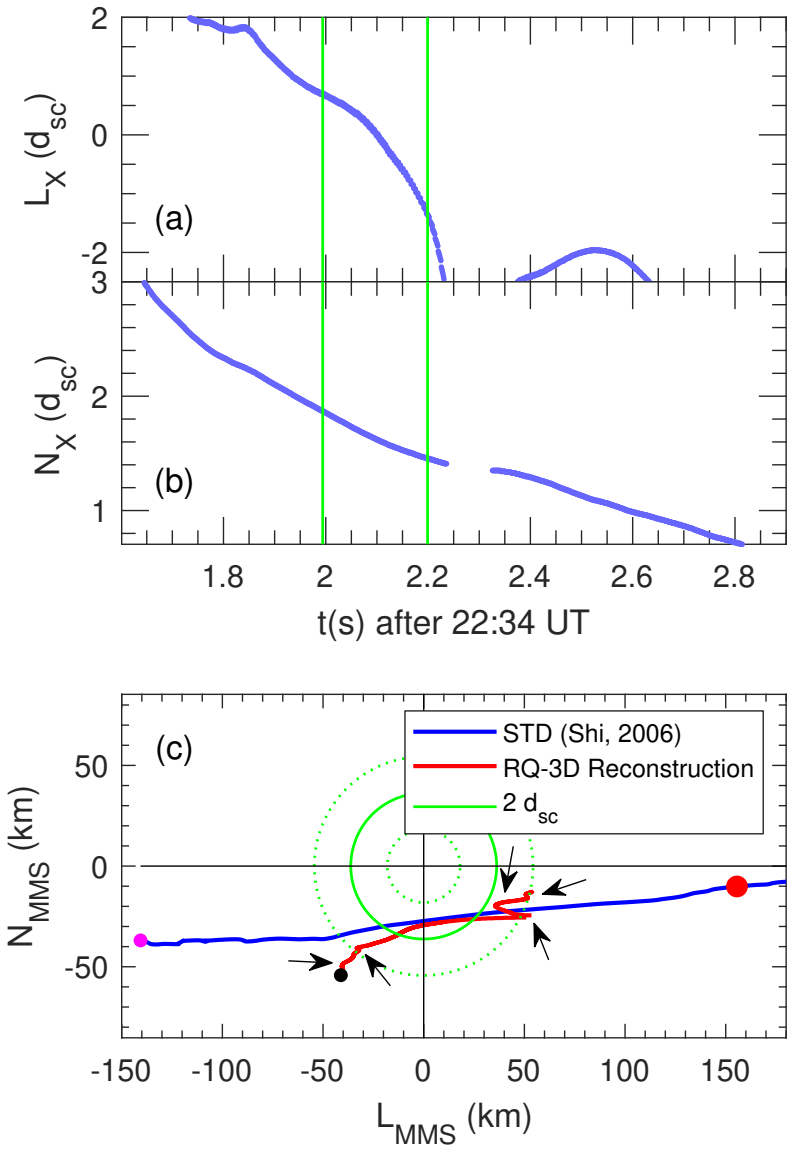

Figure 6. Motion of the spacecraft in the L-N plane. (a–b) L and N coordinates of the X line relative to the centroid of the MMS spacecraft from the RQ-3D reconstruction, (a) L_X and (b) N_X, respectively, in units of the average spacecraft spacing, d_{sc}, versus time t. (c) Path of the centroid of the MMS spacecraft through the L-N plane relative to the X line at the origin. The blue curve is from the Spatio-Temporal Difference (STD) method, and the red curve is from the reconstruction. Both paths start toward the left side of the plot and progress generally toward the right side. The black circle marks the starting point of the reconstruction path, and the black arrows represent positions along that path where there is a reversal of the L component of the velocity, v_L. The magenta circle marks the starting point of the STD path. The solid green circle is at $2d_{sc}$ from the origin.

The blue curve shows the path of the MMS spacecraft found from STD. The magenta circle at the left side of the plot shows the starting point of the path. While the STD path is shown for the entire time interval of Figures 6a and 6b, 1.6 s to 2.9 s, the points plotted within the red curve are only for the times when L_X and N_X determined from the reconstruction are within $\pm 3 d_{\rm sc}$, that is, the times for which there are blue data points shown in Figures 6a and 6b.

The STD method yields only velocities, not positions, so the position of the path is determined in the following way. For an X-like reconnection configuration at (L,N) = (0,0), B_N is expected to change sign with respect to L at $L = 0$, and B_L is expected to change sign with respect to N at $N = 0$. So the path is adjusted in the left to right direction so that the N component of the magnetic field averaged over the four spacecraft reverses at $L_{\rm MMS} = 0$ (red curve in Figure 1e at $t = 2.12$ s). This exact procedure cannot be followed to determine the vertical position of the path using B_L, because $B_{L,\rm av}$ does not reverse during our time interval (green curve in Figure 1e), indicating that the centroid of the spacecraft positions did not cross the N axis, as depicted in Figure 6c (blue curve). But MMS3 is displaced 10.1 km in the positive N direction relative to the centroid of the MMS spacecraft. (See the positions of the green circles in Figure 5b—q relative to the origin at the centroid of the spacecraft.) And MMS3 did cross the $N = 0$ line, as indicated by a reversal in B_L at 2.81 s (green curve in Figure 4a just beyond the right side of the plot). At this time the centroid of the MMS positions was at the large red circle on the right side of the plot. The STD path was adjusted in the up to down direction by requiring that $N_{\rm MMS} = 0$ was 10.1 km above the red circle.

The path of the MMS spacecraft from the reconstruction (red curve) is mostly consistent with that from STD within a distance of 2 $d_{\rm sc}$ from the X line (within the solid green circle). That is, with a slight shift of the blue curve downward, the two curves would almost exactly lie on top of each other for those parts of the curves that would be within the solid green circle. During the time that the centroid of the MMS spacecraft is within $2 d_{\rm sc}$ of the X line (2.04 s to 2.16 s, indicated by the vertical solid green lines in Figures 6a and 6b), the L and N components of the velocity based on the reconstruction were 180 km/s and 32 km/s, respectively, whereas the L and N components of the velocity based on the STD method were 236 km/s and 32 km/s, respectively. So the N components of the velocity were the same for both methods, and the L components agreed within no more than 30% (depending on how we calculate the percent difference).

Note also that both STD and the reconstruction show the largest L component of the structure velocity at about $t = 2.23$ s (based on the solid blue curve in Figure 3a and the blue curve in Figure 6a). A more precise comparison is shown in Figure 3a, where the dotted curves are the L component (cyan dotted curve) and N component (magenta dotted curve) of the structure velocity based on the motion of the X line in the polynomial reconstruction. The N components from the reconstruction is quite similar to that from STD (comparing the red solid and magenta dotted curves in Figure 3a), especially at $t = 2.0$ s and between 2.1 s and 2.2 s. There are larger differences for the L component (comparing the blue solid and cyan dotted curves in Figure 3a), but both methods yield increasingly negative velocities with respect to time, and the average values are similar.

4 Discussion

We have explained aspects of the Spatio-Temporal Difference (STD) method of *Shi et al.* [2006, 2019], and have shown how STD and the polynomial reconstruction method of *Denton et al.* [2020] can be used to determine the velocity of the magnetic structure relative to the MMS spacecraft, and then the path of the MMS spacecraft relative to the X line of the magnetic structure (Figure 6c). In order to get the path from the STD method, we had to use the time of reversal in B_N averaged over the MMS spacecraft to align the path in the L direction, and the time of reversal in B_L as observed by MMS3 to align the path in the N direction. Because the latter event occurred significantly later in time than the closest approach to the X line (2.814 s; see position of the red circle in Figure 6c), the position of the STD path probably has more uncertainty in the N direction than in the L direction. So it would not be unreasonable to shift the path from STD (blue curve in Figure 6c) slightly down to align it with the path from the reconstruction (red curve in Figure 6c). The two paths would then agree quite well for the time for which the centroid of the MMS spacecraft is within $2d_{sc}$ from the X line (within the solid green circle of Figure 6c).

The reconstruction is more likely to be accurate when the centroid of the MMS spacecraft is close to the X line, but the path calculated from STD has no such restriction. The STD and reconstruction paths agree when the centroid of the spacecraft are within a distance of $2d_{sc}$ from the X line, validating both methods when the MMS spacecraft are close to the X line. Calculating the velocity of the MMS spacecraft relative to the X line based on these two methods during the interval of time that the centroid of the spacecraft was within a distance of $2d_{sc}$ from the X line based on the reconstruction, we found that the N component of the

velocity from STD and the reconstruction agreed precisely, while the L components agreed to within no more than 30%. But there is no reason that the STD results should be less accurate when the MMS spacecraft are not close to the X line. So we conclude that the position of the X line from the reconstruction is only likely to be accurate when the centroid of the MMS spacecraft is within $2d_{sc}$ from the X line, and the STD velocity is likely to be more accurate than the reconstruction velocity when the MMS spacecraft are farther away from the X line.

As mentioned in section 3.1, *Genestreti et al.* [2018] found L, M, and N directions (their MDD-B/MVA-v_e coordinate system, coordinate system 14 in their Table A1) that varied by 40°, 39°, and 11°, respectively, from our directions. Their analysis used MDD to get the N direction, but the maximum variance direction of the electron velocity to get the L direction. They were strongly motivated by the goal of finding an M direction that yielded constant E_M. The constancy of E_M follows from Faraday's Law if the reconnection is two-dimensional (in the L-N plane) and time independent. In other words, this coordinate system was also motivated by the goal of determining M as the direction of invariance of the magnetic field. To avoid confusion with the directions based on MDD, we will indicate these directions by a ''G" subscript. Unfortunately we are not able to accurately calculate the velocity in the L_G-N_G plane using STD, because the velocity in the L_G direction would have a significant contribution from the velocity in our M direction. Then, because the gradient in our M direction is very small, the velocity in the L_G direction cannot be reliably determined. Nevertheless, we project our STD velocity onto the L_G and N_G directions to get what is probably a lower limit on these velocity components.

We also determine the velocity in the L_G-N_G plane using an RQ-3D reconstruction. Figure 7 shows the reconstructed magnetic field using the same format as Figure 5. In Figure 7, the X line moves across the field of view from right to left, as in Figure 5, but does not linger at the periphery of the plot where $L_G/d_{sc} = \pm 3$. Figure 8 is similar to Figure 6, but showing the motion of the spacecraft with respect to the L_G and N_G coordinates. The dashed blue curve in Figure 8 shows the path calculated from STD including all velocity components with eigenvalues to the right of the dotted vertical red line in Figure 2. Thus a small number of m velocity component values are included in the calculation of the L_G and N_G components of the STD velocity. The fact that the dashed blue curve in Figure 8 is slightly closer to the red curve than the blue curve is suggestive that inclusion of the miss-

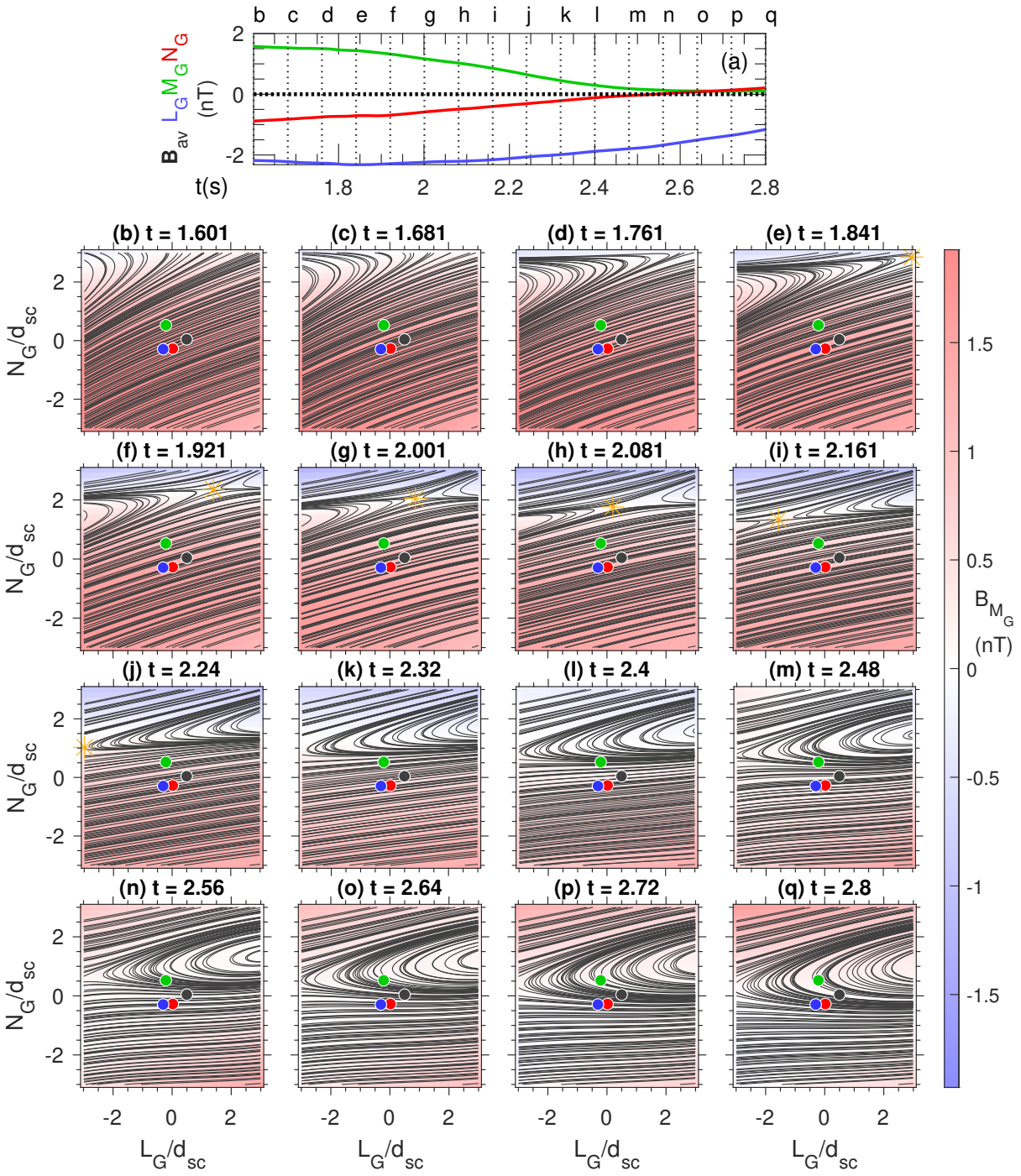

Figure 7. RQ-3D reconstruction of the magnetic field in the L_G–N_G plane at $M_G = 0$. Same as Figure 5, except showing the magnetic field in the L_G–N_G rather than L–N plane.

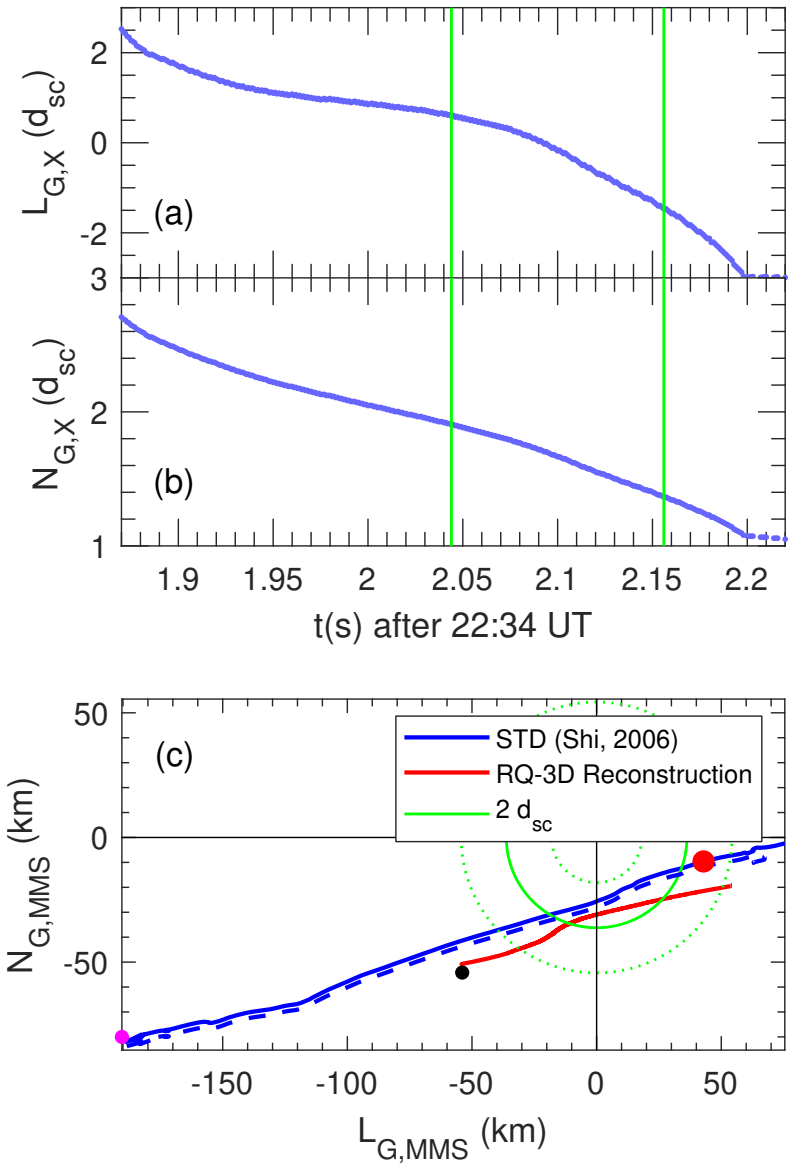

451 **Figure 8.** Motion of the spacecraft in the L_G-N_G plane. Similar to Figure 6, except showing the motion
452 using the L_G and N_G rather than L and N cordinates. The blue dashed curve in Figure 7c is found from STD
453 making use of all velocity components to the right of the red vertical dotted line in Figure 2.

Table 1. Magnetic structure velocities in the *Genestreti et al.* [2018] L_G-N_G plane

Symbol in Figure 6	θ_L^a (°)	V_{L_G} (km/s)	θ_N^b (°)	V_{N_G} (km/s)	Reference
B_{M_G}			3.7	-122	This paper, Timing with B_{M_G}
J_{M_G}			11.5	-40	This paper, Timing with J_{M_G}
S	0	-174	0	-61	This paper, STD
R	0	-333	0	-87	This paper, RQ-3D reconstruction
N	0	-250	0	-83	*Nakamura et al.* [2019]
H	5.0	-232	0.6	-59	*Hasegawa et al.* [2019]
E	10.6	-333	6.5	-72	*Egedal et al.* [2019]

[a] Angle between the L_G and reference L directions

[b] Angle between the N_G and reference N directions

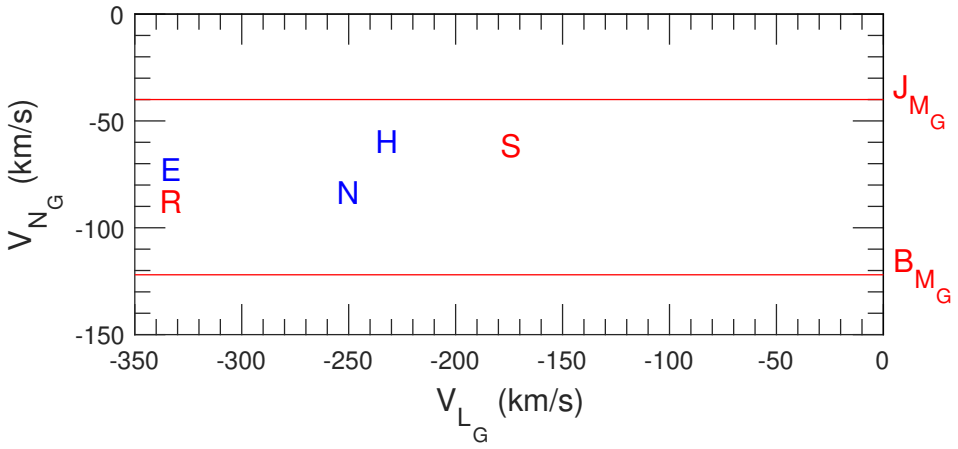

Figure 9. Magnetic structure velocities in the L_G-N_G plane. Velocities calculated in this paper (red symbols) along with velocities in various references (blue symbols), using the symbols listed in Table 1.

ing m component of velocity might possibly lead to better agreement between STD and the polynomial reconstruction.

Figure 9 compares velocity components in the L_G and N_G directions that we calculate to those that have appeared in several other references listed in Table 1. First of all, we use four spacecraft timing analysis using B_{M_G} and J_{M_G} to determine the N_G components of the velocity only [*Dunlop and Woodward*, 1998]. The angle between the timing normal and the Genestreti et al. N_G direction, θ_N, is small in both cases, as shown in Table 1. Therefore

the timing analysis is approximately giving the velocity in the N direction. But the results differ greatly depending on the quantity used, as indicated by -122 km/s value found using B_{M_G} and the -40 km/s value found using J_{M_G} (see the red horizontal lines in Figure 9). The velocity found from projection of our STD velocity onto the L_G and N_G directions is indicated in Table 1 and Figure 9 by the "S" symbol (red in Figure 9), and for the reconstruction using the "R" symbol (red in Figure 9). Velocities from *Nakamura et al.* [2019], *Hasegawa et al.* [2019], and *Egedal et al.* [2019] are indicated in Table 1 and Figure 9 respectively by the "N", "H", and "E" symbols (blue in Figure 9).

The N_G components from STD and RQ-3D and the three papers referenced are fairly consistent (letter symbols in Figure 9), and lie between the values from the timing analysis (red horizontal lines in Figure 9). The L_G velocity component from STD is significantly less in magnitude than the other estimates, probably owing to the problem of evaluating the STD velocity component in the M_G direction, mentioned previously. The L_G velocity component from the reconstruction is equal to that from the *Egedal et al.* [2019] reference, and this estimate has the largest magnitude.

In the L-N coordinate system based on Minimum Directional Derivative (MDD) analysis, the STD and reconstruction velocities agree fairly well (within about 30%), at least when the centroid of the MMS spacecraft is within $2d_{\mathrm{sc}}$ of the X line. This would appear to roughly validate both of these methods ("roughly" because the L components of the velocities in Figure 3a are certainly not exactly the same). Also, the L coordinate in Figure 5 based on MDD seems to be much better aligned with the current sheet than that in Figure 7.

There are some differences in results with different averaging of the data. If the data is smoothed over less than 0.5 s, the reconstruction yields some additional time dependent behavior. With 0.3 s smoothing, there appears to be coalescence-like merging of a plasmoid with the large scale island. Because of the shape of the merging plasmoid (elongated in the L direction), we do not regard this short timescale behavior to be realistic. (It would not be energetically favorable.) If the data is smoothed over a larger time, some of the intermediate eigenvalues become even lower than those in Figure 2. But the values of λ_l/λ_0 are still greater than unity for $t < 2.35$ s. And there is still no increase in the intermediate gradient (l) velocity component as the eigenvalue decreases such as occurs for the minimum gradient component (green dots) in Figure 2 for $\lambda_m/\lambda_0 < 0.1$.

Genestreti et al. [2018], however, argued that relatively small magnetic field calibration errors could significantly alter the MDD directions. In particular, their Figure 8 suggests that calibration errors for **B** of order 0.05 nT can cause errors in the L and M directions with typical values of 10°, but ranging from small values to 20°. There is definitely an inconsistency between the M component directions based on the minimum gradient from MDD or the constancy of E_M, used to validate Genestreti et al.'s coordinate system. This is because the argument that E_M should be constant is based on supposed invariance of **B** in the M direction, which should be the MDD minimum gradient direction. Genestreti et al. looked for coordinate systems for which the small value E_M was not dependent on the larger E_N. They found that E_M in the MDD coordinate system varied with E_N, and on average was negative, implying that reconnection would not be occurring. On the other hand, $E_{M,G}$ was relatively independent of $E_{N,G}$. Other results favoring a coordinate system similar to that of Genestreti et al. are the optimal coordinate system for Electron MHD (EMHD) reconstruction [*Hasegawa et al.*, 2019] and the good correlation between **B** and the electron velocity as the magnetic field rotates from the L to M direction [*Le et al.*, 2010] found in the simulation of this event by *Egedal et al.* [2019]. This rotation is consistent with the wave reconnection dynamics first described by *Mandt et al.* [1994], and then later generalized to electron scale structures [*Le et al.*, 2010, 2013].

Of course, evaluating the coordinate system based on the constancy of E_M also involves assumptions, two dimensionality, no time dependence, and accurate calculation of the electric field. But we cannot rule out the possibility that magnetic field calibration errors are affecting the inferred magnetic structure (like the orientation of the current sheet in Figures 5) and our results for $V_{\mathrm{str},L}$. For that reason, we also calculated the reconstruction velocity in Genestreti et al.'s coordinate system. The gradient in the N direction, and hence $V_{\mathrm{str},N}$, however, is much better determined than that in the L direction, and at any rate, the N directions of both coordinate systems were fairly similar, differing by 11°.

Even if the minimum magnetic field gradient direction was determined correctly, results by *Denton et al.* [2016a, 2018] indicate that the minimum gradient direction can be the L direction determined to have maximum variation in the magnetic field, which we usually associate with the reconnection magnetic field. Perhaps some sort of reconciliation for the difference in the M direction based on the magnetic field gradient or constancy in the electric field results from the fact that the magnetic field geometry is in some sense approximately one dimensional based on the relative size of the maximum and intermediate gradient eigen-

values in Figure 1a. From that perspective, there are two directions of relatively small spatial inhomogeneity relative to that of the N direction. At any rate, it seems that different kinds of data align themselves better to different coordinate systems.

Both STD and the reconstruction would work better if the spacecraft spacing were somewhat larger, so that the gradients would be better determined and λ_k would be larger relative to λ_0. (The spacing should be not so much larger that the spacecraft are sampling different structures.) Both the STD and reconstruction results strongly depend on the observed gradients in the magnetic field components. It is encouraging, however, that the STD L component of the velocity is affected most strongly by the variation of B_M and B_L, and less so (though not insignificantly) by the variation of B_N (Figure 3b), whereas the L component of the velocity from the polynomial reconstruction is affected mostly by the spatial variation in B_N (since the X line is at the reversal in B_N). Also our estimate for $\mathbf{V}_{\rm str}$ in the *Genestreti et al.* [2018] coordinate system based on the reconstruction did not differ greatly from other velocity estimates (Figure 9).

Acknowledgments

Work at Dartmouth College was supported by NASA grant 80NSSC19K0254. The MMS data set is available on-line at https://lasp.colorado.edu/mms/sdc/public/links/.

A: Derivation of STD structure velocity

Expressing (2) as a matrix equation,

$$\mathbf{B}_{dt} = -\mathbf{V}_{\rm str} \cdot \mathbf{G}, \tag{A.1}$$

where $\mathbf{B}_{dt}$ and $\mathbf{V}_{\rm str}$ are row vectors, and

$$\mathbf{G} = \nabla \mathbf{B} \tag{A.2}$$

is a matrix with the partial spatial derivatives varying along the column direction.

Now we multiply (A.1) by the transpose of G, $\mathbf{G}^T$, to get

$$\mathbf{B}_{dt} \cdot \mathbf{G}^T = -\mathbf{V}_{\rm str} \cdot \mathbf{G} \cdot \mathbf{G}^T = -\mathbf{V}_{\rm str} \cdot \mathbf{M}_{\rm G}, \tag{A.3}$$

where

$$\mathbf{M}_{\rm G} = \mathbf{G} \cdot \mathbf{G}^T. \tag{A.4}$$

Assume that we have used MDD to get the local time dependent gradient directions, n, l and m. At each time, we define a rotation matrix, $\mathbf{M}$, that has the eigenvectors along the columns.

Now we transform to the local eigenvector frame by multiplying (A.3) by $\mathbf{M}$ on the right and using $\mathbf{M} \cdot \mathbf{M}^T = I$, where I is the identity matrix, to get

$$\mathbf{B}_{dt} \cdot \mathbf{M} \cdot \mathbf{M}^T \cdot \mathbf{G}^T \cdot \mathbf{M} = -\mathbf{V}_{\rm str} \cdot \mathbf{M} \cdot \mathbf{M}^T \cdot \mathbf{M}_{\rm G} \cdot \mathbf{M}, \tag{A.5}$$

or

$$\mathbf{B_{dt}} \cdot \mathbf{G}^{\boldsymbol{T}} = -\mathbf{V_{str}} \cdot \mathbf{M_G}. \tag{A.6}$$

Then, as described by *Shi et al.* [2006], we can solve for $\mathcal{V}_{\rm str}$ in closed form (equation (3)) using the fact that $\mathcal{M}_{\rm G}$ is diagonal in the local MDD coordinate system l-m-n with the gradient eigenvalues, λ_k.

B: Model current density

To calculate the current density $\mu_0\mathbf{J}$ for the Reduced Quadratic model of *Denton et al.* [2020], we simply take the curl of equations (6–8). For instance, $\mu_0 J_l = \partial B_n/\partial m - \partial B_m/\partial n$.

The result is:

$$\mu_0 J_l = \frac{\partial B_n}{\partial m} - \left(\frac{\partial B_m}{\partial n} + \frac{\partial^2 B_m}{\partial n^2} n + \frac{\partial^2 B_m}{\partial n \partial l} l\right) \tag{B.1}$$

$$\mu_0 J_m = \frac{\partial B_l}{\partial n} + \frac{\partial^2 B_l}{\partial n^2} n - \left(\frac{\partial B_n}{\partial l} + \frac{\partial^2 B_n}{\partial l^2} l\right) \tag{B.2}$$

$$\mu_0 J_n = \frac{\partial B_m}{\partial l} + \frac{\partial^2 B_m}{\partial n \partial l} n + \frac{\partial^2 B_m}{\partial l^2} l - \frac{\partial B_l}{\partial m} \tag{B.3}$$

Note that $\mu_0 \mathbf{J}$ is at most linear with respect to l and n since the curl operation involves a derivative.

References

Alm, L., M. R. Argall, R. B. Torbert, C. J. Farrugia, J. L. Burch, R. E. Ergun, C. T. Russell, R. J. Strangeway, Y. V. Khotyaintsev, P. A. Lindqvist, G. T. Marklund, B. L. Giles, and J. Shuster (2017), EDR signatures observed by MMS in the 16 October event presented in a 2-D parametric space, *J. Geophys. Res.*, *122*(3), 3262–3276, doi:10.1002/2016ja023788.

Argall, M. R., D. Fischer, O. Le Contel, L. Mirioni, R. B. Torbert, I. Dors, M. Chutter, N. J., R. Strangeway, W. Magnes, and C. T. Russell (2018), The Fluxgate-Searchcoil Merged (FSM) Magnetic Field Data Product for MMS, *ArXiv*, doi: https://arxiv.org/abs/1809.07388.

Burch, J. L., T. E. Moore, R. B. Torbert, and B. L. Giles (2015), Magnetospheric Multiscale Overview and Science Objectives, *Space Science Reviews*, doi:10.1007/s11214-015-0164-9.

Denton, R. E., B. U. O. Sonnerup, H. Hasegawa, T. D. Phan, C. T. Russell, R. J. Strangeway, B. L. Giles, D. Gershman, and R. B. Torbert (2016a), Motion of the MMS spacecraft relative to the magnetic reconnection structure observed on 16 October 2015 at 1307 UT, *Geophys. Res. Lett.*, *43*(11), 5589–5596, doi:10.1002/2016gl069214.

Denton, R. E., B. U. O. Sonnerup, H. Hasegawa, T. D. Phan, C. T. Russell, R. J. Strangeway, B. L. Giles, and R. B. Torbert (2016b), Reconnection guide field and quadrupolar structure observed by MMS on 16 October 2015 at 1307 UT, *J. Geophys. Res.*, *121*(10), 9880–9887, doi:10.1002/2016ja023323.

596 Denton, R. E., B. U. O. Sonnerup, C. T. Russell, H. Hasegawa, T. D. Phan, R. J. Strange-
597 way, B. L. Giles, R. E. Ergun, P. A. Lindqvist, R. B. Torbert, J. L. Burch, and S. K.
598 Vines (2018), Determining L-M-N Current Sheet Coordinates at the Magnetopause
599 From Magnetospheric Multiscale Data, *J. Geophys. Res.*, *123*(3), 2274–2295, doi:
600 10.1002/2017ja024619.

601 Denton, R. E., R. B. Torbert, H. Hasegawa, I. Dors, K. J. Genestreti, M. R. Argall, D. Gersh-
602 man, O. Le Contel, J. L. Burch, C. T. Russell, R. J. Strangeway, B. L. Giles, and D. Fischer
603 (2020), Polynomial reconstruction of the reconnection magnetic field observed by mul-
604 tiple spacecraft, *JOURNAL OF GEOPHYSICAL RESEARCH-SPACE PHYSICS*, *125*(2),
605 doi:10.1029/2019JA027481.

606 Dunlop, M. W., and T. I. Woodward (1998), Multi-Spacecraft Discontinuity Analysis:
607 Orientation and Motion, in *Analysis Methods for Multi-Spacecraft Data*, edited by
608 G. Paschmann and P. Daly, pp. 271–306, International Space Science Institute, SR-001,
609 Bern Switzerland.

610 Egedal, J., J. Ng, A. Le, W. Daughton, B. Wetherton, J. Dorelli, D. Gershman, and
611 A. Rager (2019), Pressure tensor elements breaking the frozen-in law during re-
612 connection in earth's magnetotail, *PHYSICAL REVIEW LETTERS*, *123*(22), doi:
613 {10.1103/PhysRevLett.123.225101}.

614 Fischer, D., W. Magnes, C. Hagen, I. Dors, M. W. Chutter, J. Needell, R. B. Torbert,
615 O. Le Contel, R. J. Strangeway, G. Kubin, A. Valavanoglou, F. Plaschke, R. Nakamura,
616 L. Mirioni, C. T. Russell, H. K. Leinweber, K. R. Bromund, G. Le, L. Kepko, B. J. An-
617 derson, J. A. Slavin, and W. Baumjohann (2016), Optimized merging of search coil and
618 fluxgate data for MMS, *Geoscientific Instrumentation Methods and Data Systems*, *5*(2),
619 521–530, doi:10.5194/gi-5-521-2016.

620 Genestreti, K. J., T. K. M. Nakamura, R. Nakamura, R. E. Denton, R. B. Torbert, J. L. Burch,
621 F. Plaschke, S. A. Fuselier, R. E. Ergun, B. L. Giles, and C. T. Russell (2018), How accu-
622 rately can we measure the reconnection rate E_M for the MMS diffusion region event of
623 2017-07-11?, *J. Geophys. Res.*, *123*.

624 Hasegawa, H., R. E. Denton, R. Nakamura, K. J. Genestreti, T. K. M. Nakamura, K. J.
625 Hwang, T. D. Phan, R. B. Torbert, L. Burch, B. L. Giles, D. J. Gershman, C. T. Russell,
626 R. J. Strangeway, P. A. Lindqvist, Y. V. Khotyaintsev, R. E. Ergun, N. Kitamura, and
627 Y. Saito (2019), Reconstruction of the Electron Diffusion Region of Magnetotail Recon-
628 nection seen by the MMS Spacecraft on 11 July 2017, *J. Geophys. Res.*, *124*(1), 122–138,

doi:10.1029/2018ja026051.

Hesse, M., T. Neukirch, K. Schindler, M. Kuznetsova, and S. Zenitani (2011), The Diffusion Region in Collisionless Magnetic Reconnection, *Space Science Reviews*, *160*(1-4), 3–23, doi:10.1007/s11214-010-9740-1.

Hesse, M., N. Aunai, J. Birn, P. Cassak, R. E. Denton, J. F. Drake, T. Gombosi, M. Hoshino, W. Matthaeus, D. Sibeck, and S. Zenitani (2014), Theory and Modeling for the Magnetospheric Multiscale Mission, *Space Science Reviews*, doi:10.1007/s11214-014-0078-y.

Le, A., J. Egedal, W. Fox, N. Katz, A. Vrublevskis, W. Daughton, and J. F. Drake (2010), Equations of state in collisionless magnetic reconnection, *Phys. Plasmas*, *17*(5), doi:10.1063/1.3309425.

Le, A., J. Egedal, O. Ohia, W. Daughton, H. Karimabadi, and V. S. Lukin (2013), Regimes of the Electron Diffusion Region in Magnetic Reconnection, *Phys. Rev. Lett.*, *110*(13), doi:10.1103/PhysRevLett.110.135004.

Le Contel, O., P. Leroy, A. Roux, C. Coillot, D. Alison, A. Bouabdellah, L. Mirioni, L. Meslier, A. Galic, M. C. Vassal, R. B. Torbert, J. Needell, D. Rau, I. Dors, R. E. Ergun, J. Westfall, D. Summers, J. Wallace, W. Magnes, A. Valavanoglou, G. Olsson, M. Chutter, J. Macri, S. Myers, S. Turco, J. Nolin, D. Bodet, K. Rowe, M. Tanguy, and B. de la Porte (2016), The Search-Coil Magnetometer for MMS, *Space Science Reviews*, *199*(1-4), 257–282, doi:10.1007/s11214-014-0096-9.

Mandt, M. E., R. E. Denton, and J. F. Drake (1994), TRANSITION TO WHISTLER MEDIATED MAGNETIC RECONNECTION, *Geophys. Res. Lett.*, *21*(1), 73–76, doi:10.1029/93gl03382.

Manuzzo, R., G. Belmont, L. Rezeau, F. Califano, and R. E. Denton (2019), Crossing of Plasma Structures by Spacecraft: A Path Calculator, *JOURNAL OF GEOPHYSICAL RESEARCH-SPACE PHYSICS*, *124*(12), 10,119–10,140, doi:10.1029/2019JA026632.

Nakamura, R., K. J. Genestreti, T. Naltamora, W. Baumjohann, A. Varsani, T. Nagai, N. Bessho, J. L. Burch, R. E. Denton, J. P. Eastwood, R. E. Ergun, D. J. Gershman, A. L. Giles, I. Hasegaw, M. Hesse, P.-A. Lindqvist, H. T. Russell, U. E. Stawarz, R. J. Strangeway, and R. B. Torber (2019), Structure of the Current Sheet in the 11 July 2017 Electron Diffusion Region Event, *Journal of Geophysical Research-Space Physics*, *124*(2), 1173–1186, doi:10.1029/2018JA026028.

Pollock, C., T. Moore, A. Jacques, J. Burch, U. Gliese, Y. Saito, T. Omoto, L. Avanov, A. Barrie, V. Coffey, J. Dorelli, D. Gershman, B. Giles, T. Rosnack, C. Salo, S. Yokota,

M. Adrian, C. Aoustin, C. Auletti, S. Aung, V. Bigio, N. Cao, M. Chandler, D. Chornay, K. Christian, G. Clark, G. Collinson, T. Corris, A. D. L. Santos, R. Devlin, T. Diaz, T. Dickerson, C. Dickson, A. Diekmann, F. Diggs, C. Duncan, A. Figueroa-Vinas, C. Firman, M. Freeman, N. Galassi, K. Garcia, G. Goodhart, D. Guererro, J. Hageman, J. Hanley, E. Hemminger, M. Holland, M. Hutchins, T. James, W. Jones, S. Kreisler, J. Kujawski, V. Lavu, J. Lobell, E. LeCompte, A. Lukemire, E. MacDonald, A. Mariano, T. Mukai, K. Narayanan, Q. Nguyan, M. Onizuka, W. Paterson, S. Persyn, B. Piepgrass, F. Cheney, A. Rager, T. Raghuram, A. Ramil, L. Reichenthal, H. Rodriguez, J. Rouzaud, A. Rucker, Y. Saito, M. Samara, J.-A. Sauvaud, D. Schuster, M. Shappirio, K. Shelton, D. Sher, D. Smith, K. Smith, S. Smith, D. Steinfeld, R. Szymkiewicz, K. Tanimoto, J. Taylor, C. Tucker, K. Tull, A. Uhl, J. Vloet, P. Walpole, S. Weidner, D. White, G. Winkert, P.-S.Yeh, and M. Zeuch (2016), Fast Plasma Investigation for Magnetospheric Multiscale, *Space Science Reviews*, doi:10.1007/s11214-016-0245-4.

Robert, P., M. W. Dunlop, A. Roux, and G. Chanteur (1998), Accuracy of current density determination, in *Analysis Methods for Multi-Spacecraft Data*, edited by G. Paschmann and P. Daly, pp. 395–418, International Space Science Institute, SR-001, Bern Switzerland.

Russell, C. T., B. J. Anderson, W. Baumjohann, K. R. Bromund, D. Dearborn, D. Fischer, G. Le, H. K. Leinweber, D. Leneman, W. Magnes, J. D. Means, M. B. Moldwin, R. Nakamura, D. Pierce, F. Plaschke, K. M. Rowe, J. A. Slavin, R. J. Strangeway, R. Torbert, C. Hagen, I. Jernej, A. Valavanoglou, and I. Richter (2016), The Magnetospheric Multiscale Magnetometers, *Space Science Reviews*, doi:10.1007/s11214-014-0057-3.

Shi, Q. Q., Z. Y. Pu, H. Zhang, S. Y. Fu, C. J. Xiao, Q. G. Zong, T. A. Fritz, and Z. X. Liu (2005), Simulation studies of high-latitude magnetospheric boundary dynamics, *Surveys in Geophysics*, *26*(1-3), 369–386, doi:10.1007/s10712-005-1900-6.

Shi, Q. Q., C. Shen, M. W. Dunlop, Z. Y. Pu, Q. G. Zong, Z. X. Liu, E. Lucek, and A. Balogh (2006), Motion of observed structures calculated from multi-point magnetic field measurements: Application to Cluster, *Geophys. Res. Lett.*, *33*(8), doi:10.1029/2005gl025073.

Shi, Q. Q., A. M. Tian, S. C. Bai, H. Hasegawa, A. W. Degeling, Z. Y. Pu, M. Dunlop, R. L. Guo, S. T. Yao, Q. G. Zong, Y. Wei, X. Z. Zhou, S. Y. Fu, and Z. Q. Liu (2019), Dimensionality, Coordinate System and Reference Frame for Analysis of In-Situ Space Plasma and Field Data, *Space Science Reviews*, *215*(4), doi:10.1007/s11214-019-0601-2.

Sonnerup, B. O. U. (1979), Magnetic field reconnection, in *Solar System Plasma Physics*, vol. 3 (A79-53667 24-46), pp. 45–108, North-Holland Publishing Co., Amsterdam.

Sonnerup, B. U., and L. J. Cahill (1967), Magnetopause Structure and Attitude from Explorer 12 Observations, *Journal of Geophysical Research*, *72*(1).

Sonnerup, B. U. O., and M. Scheible (1998), Minimum and maximum variance analysis, in *Analysis Methods for Multi-Spacecraft Data*, edited by G. Paschmann and P. Daly, pp. 185–220, International Space Science Institute, SR-001, Bern Switzerland.

Torbert, R. B., J. L. Burch, T. D. Phan, M. Hesse, M. R. Argall, J. Shuster, R. E. Ergun, L. Alm, R. Nakamura, K. J. Genestreti, D. J. Gershman, W. R. Paterson, D. L. Turner, I. Cohen, B. L. Giles, C. J. Pollock, S. Wang, L.-J. Chen, J. E. Stawarz, J. P. Eastwood, K. J. Hwang, C. Farrugia, I. Dors, H. Vaith, C. Mouikis, A. Ardakani, B. H. Mauk, S. A. Fuselier, C. T. Russell, R. J. Strangeway, T. E. Moore, J. F. Drake, M. A. Shay, Y. V. Khotyaintsev, P.-A. Lindqvist, W. Baumjohann, F. D. Wilder, N. Ahmadi, J. C. Dorelli, L. A. Avanov, M. Oka, D. N. Baker, J. F. Fennell, J. B. Blake, A. N. Jaynes, O. Le Contel, S. M. Petrinec, B. Lavraud, and Y. Saito (2018a), Electron-scale dynamics of the diffusion region during symmetric magnetic reconnection in space, *Science*, *362*(6421), 1391–+, doi:10.1126/science.aat2998.

Torbert, R. B., J. L. Burch, M. R. Argall, C. J. Farrugia, I. Dors, D. Payne, K. J. Genestreti, A. J. Rogers, R. J. Strangeway, T. Phan, R. Ergun, Y. V. Khotyainstsev, and B. L. Giles (2018b), Energetics within Selected MMS Encounters of Electron Diffusion Regions, AGU, Abstract SM33A-02 presented at the 2018 Fall Meeting, Washington DC, 10-14 Dec.

Torbert, R. B., I. Dors, M. R. Argall, K. J. Genestreti, J. L. Burch, C. J. Farrugia, T. G. Forbes, B. L. Giles, and R. J. Strangeway (2020), A New Method of 3-D Magnetic Field Reconstruction, *Geophysical Research Letters*, *47*(3), e2019GL085,542, doi:10.1029/2019GL085542.

Vasyliunas, V. (1975), Theoretical models of magnetic-field line merging .1., *Reviews Of Geophysics*, *13*(1), 303–336, doi:10.1029/RG013i001p00303.

Yao, S. T., Q. Q. Shi, Z. Y. Li, X. G. Wang, A. M. Tian, W. J. Sun, M. Hamrin, M. M. Wang, T. Pitkanen, S. C. Bai, X. C. Shen, X. F. Ji, D. Pokhotelov, Z. H. Yao, T. Xiao, Z. Y. Pu, S. Y. Fu, Q. G. Zong, A. De Spiegeleer, W. Liu, H. Zhang, and H. Reme (2016), Propagation of small size magnetic holes in the magnetospheric plasma sheet, *J. Geophys. Res.*, *121*(6), 5510–5519, doi:10.1002/2016ja022741.

Yao, S. T., Q. Q. Shi, R. L. Guo, Z. H. Yao, A. M. Tian, A. W. Degeling, W. J. Sun, J. Liu, X. G. Wang, Q. G. Zong, H. Zhang, Z. Y. Pu, L. H. Wang, S. Y. Fu, C. J. Xiao, C. T. Russell, B. L. Giles, Y. Y. Feng, T. Xiao, S. C. Bai, X. C. Shen, L. L. Zhao, and H. Liu (2018), Magnetospheric Multiscale Observations of Electron Scale Magnetic Peak, *Geophys. Res. Lett.*, *45*(2), 527–537, doi:10.1002/2017gl075711.